

# Microstructured Active Phosphate Glass Fibers for Fiber Lasers

Axel Schülzgen, Li Li, Xiushan Zhu, Valery L. Temyanko, and Nasser Peyghambarian, *Member, IEEE, Member, OSA*

(Invited Paper)

**Abstract**—In this paper, we report on progress in design and fabrication of microstructured fibers made of phosphate glasses. The combination of microstructured large core fibers and very high solubility of rare-earth ions leads to improved performance of compact fiber lasers with single-frequency emission at power levels above 2 W. Microstructure-induced birefringence in active phosphate fibers is also demonstrated as well as the possibility of birefringence due to subwavelength dielectric structures inside the fiber core.

**Index Terms**—Optical fiber devices, optical fiber fabrication, optical fiber lasers, optical fiber materials, optical fiber polarization.

## I. INTRODUCTION

THE invention of microstructured optical fiber (MOF) [1] has opened new avenues for the design of fiber optic components and devices. The most widely applied types of MOF feature a cladding with a periodic pattern of different dielectrics. This pattern runs through the length of the fiber and results in unconventional guiding characteristics. The microstructure enables to select the wavelengths of light that can propagate with low losses and also determines the characteristics of the supported modes in terms of field distribution, propagation constant, and dispersion [2]. Examples of widely used MOF designs include fibers that support endless single-mode guidance in large area solid cores [3], [4], fibers with hollow cores featuring photonic band gap guiding [5], and fibers with extremely small cores for nonlinear optics and sensing applications [2].

Most MOF are fabricated from a single material and the microstructure is formed by removing material from the fiber preform. Recently, fibers with different glass materials have also attracted interest mainly due to their application in lasers and amplifiers [6]. Almost all glass MOF are based on silica and attempts to use nonsilica glasses are still rare; some examples

Manuscript received January 20, 2009; revised April 06, 2009. First published May 08, 2009; current version published May 29, 2009. This work was supported by the National Sciences Foundation under Grant 0725479 and by the Arizona Technology and Research Initiative Fund.

A. Schülzgen, X. Zhu, V. L. Temyanko, and N. Peyghambarian are with the College of Optical Sciences, University of Arizona, Tucson, AZ 85721 USA (e-mail: axel@optics.arizona.edu; xszhu@email.arizona.edu; vtemyanko@optics.arizona.edu; nnp@u.arizona.edu).

L. Li was with College of Optical Sciences, University of Arizona, Tucson, AZ 85721 USA. He is now with TIPD LLC, Tucson, AZ 85705 USA (e-mail: lili@tipd.com).

Color versions of one or more of the figures in this paper are available online at <http://ieeexplore.ieee.org>.

Digital Object Identifier 10.1109/JLT.2009.2022476

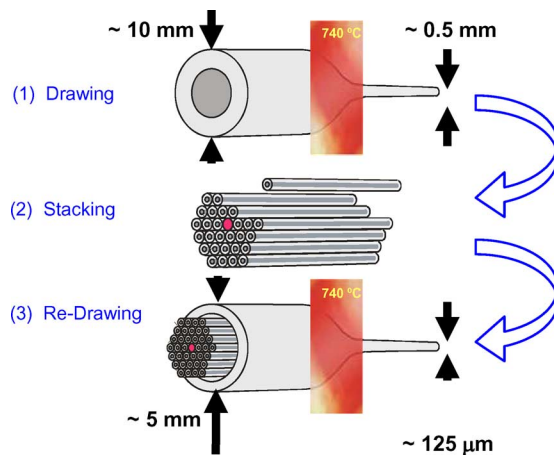


Fig. 1. Multiple drawing technique for fabrication of microstructured fiber.

are given in [7]–[9]. Although propagation losses in nonsilica MOF are typically higher, they can offer special properties that might be advantageous for applications including transparency at other wavelength particularly in the infrared region, high optical nonlinearity, and high solubility of rare-earth ions.

Here we will present our efforts to utilize microstructures in optical fibers based on phosphate glasses. Over the past years, we developed techniques to fabricate phosphate glass fiber that incorporate a variety of structures including air holes of different sizes and shapes, highly doped solid cores, and also cores consisting of different glasses that can be arranged in suitable patterns to achieve specific properties. We show that phosphate MOFs can be utilized to improve the performance of single-frequency fiber lasers and also to introduce birefringent phosphate fiber components with different designs that, e.g., can be utilized to control fiber laser polarization.

## II. FABRICATION OF PHOSPHATE GLASS MOF

Stack-and-draw and extrusion are the main techniques to fabricate MOF. Because of its high versatility and flexibility, we focus on the stacking method for the fabrication of phosphate glass MOF. Although the general scheme is very similar to stacking of silica MOF, different material properties require modifications of the various processing steps to master the challenge of fabricating high-quality phosphate glass MOF. Fig. 1 illustrates the procedure of our MOF fabrication. In a first step, several preforms are fabricated by glass machining and polishing. These preforms can be solid single-material

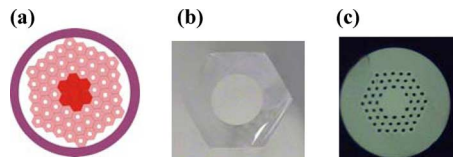


Fig. 2. Design (a) and experimental realization (c) of a microstructured fiber with large area active core (right). (b) Hexagonal unit used to assemble the cladding with air holes.

units, glass pieces with air holes, or rod-in tube units made of two different phosphate glasses. Glass types that we apply include both undoped and doped multicomponent phosphate glasses. During the first drawing process the preform units are drawn to outer diameters of  $\sim 5$  mm. This process is followed by stacking segments of 10–20-cm length to create the desired pattern of the fiber cross section. The resulting stack is typically inserted into another glass tube that forms an outer cladding after the second drawing process. The final MOF is usually made compatible to standard fiber optic components with an outer fiber diameter of  $125 \mu\text{m}$ . Note that phosphate glass is softer than silica and typical drawing temperature are relatively low in the range of  $700^\circ\text{C}$ – $800^\circ\text{C}$ . If necessary, the stacking and redrawing cycle can be repeated another time to create fiber incorporating structures with subwavelength feature sizes. An example of such a fiber will be given in Section IV-B, where the core itself contains a pattern resulting in optical birefringence of the fundamental mode.

In Fig. 2, a specific example of an active MOF with highly doped large mode area core is presented. Fig. 2(a) shows the fiber design with an arrangement including seven central doped units, three layers of undoped glasses units in the inner cladding with air holes arranged on a triangular lattice, and an outer cladding made of a third glass with lower refractive index. As shown in Fig. 2(b), we used hexagons as the shape of our original “unit cells” because of their stacking and space filling properties. For the inner cladding, holes have been drilled into hexagons of undoped phosphate glass. Fig. 2(c) is a microscope image of the facet of the fabricated phosphate glass MOF that has been applied as gain segments in efficient compact fiber lasers.

### III. FIBER LASERS WITH ACTIVE MICROSTRUCTURED PHOSPHATE FIBER

MOF with solid cores surrounded by claddings that contain several layers of air holes are good candidates for gain fiber in fiber amplifiers and lasers. In particular, the possibility of endless single-mode guidance provides a direct avenue towards single-mode fiber with large mode areas. For amplifiers and lasers large mode areas are highly desirable since they lead to improvements in absorption of cladding-launched multimode pump light and to a reduction in detrimental nonlinear effects. First, MOF fiber lasers used silica as the base material [6], [10] while we apply phosphate glass MOF to utilize the extraordinary rare-earth solubility and its corresponding high light absorption and amplification per unit length [11]–[14].

The MOF approach to gain fiber also offers a large number of design parameters including at least three refractive indices, the diameter and pitch of the air holes, as well as the number of

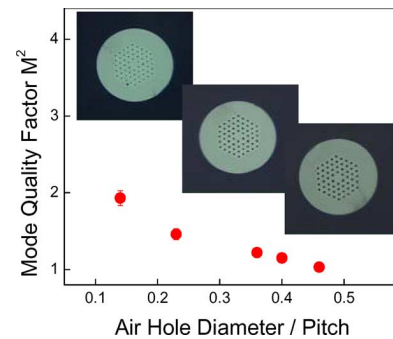


Fig. 3. Dependence of the mode quality factor of various fiber lasers on the design (ratio of air hole diameter to pitch) of the active phosphate glass MOF. Dots are experimental data of the fiber laser mode quality using five different active MOFs where the air hole sizes have been changed while all other geometrical parameters are identical. The data agree well with calculated values for the fundamental mode [11]. Insets show examples of active MOF cross sections.

unit cells that form the doped core. The MOF design parameters have a large influence on the performance of fiber lasers. As an example the dependence of the mode quality factor  $M^2$  on the ratio between air hole diameter and pitch (i.e., the distance between the centers of neighboring air holes) is shown in Fig. 3. These active phosphate MOFs utilize the classical design, where one central unit is replaced by a solid doped core [6], [11], [12] as illustrated by the pictures of the fiber facets in the insets. The cores were doped at levels of  $1.1 \times 10^{26} \text{ Er}^{3+}$  ions/ $\text{m}^3$  and  $2.2 \times 10^{26} \text{ Yb}^{3+}$  ions/ $\text{m}^3$ . Doping inevitably introduces an index difference between core and cladding glass. For the presented active fibers, the core glass index is smaller than the cladding glass index by  $\sim 7 \times 10^{-4}$  resulting in antiguiding properties if the holes in the cladding are closed. This index difference also facilitates relatively small  $M^2$  values throughout the range of  $d/\Lambda$  ratios considered in the experiments. All lasers have active fiber segments that are 11 cm long and the data were taken at broadband ( $\sim 4$  nm) operation at a center wavelength of  $1.535 \mu\text{m}$ . The data demonstrate the deteriorating mode quality with reduced air hole to pitch ratio that is caused by strong deviations of the mode shape from a desirable Gaussian mode. Although this is a demonstration of the design flexibility of active MOF, we found that a different design, namely, the replacement of seven units in the MOF center by doped solid glass [15], is best suited for active fiber segments in compact phosphate glass fiber lasers [13].

To demonstrate the advantages of the MOF concept, we directly compare the performance of two almost identical single-frequency lasers in Fig. 4(a): one with a conventional step-index active fiber [16] and the other with an active MOF [14]. The cavity geometry of both single-frequency phosphate glass fiber lasers is basically identical and shown in Fig. 4(b). The 976-nm pump light from multimode semiconductor laser is delivered through the end facet with a dielectric coating of multiple  $\text{SiO}_2$  and  $\text{Ta}_2\text{O}_5$  layers that transmits the pump light but acts as a high reflector at the operation wavelength of both lasers ( $1.534 \mu\text{m}$ ). The exact lasing wavelength is determined by the reflection spectrum of the narrowband fiber Bragg grating (FBG). The doping levels in the active fiber have been kept the same for both active fibers at  $1.6 \times 10^{26} \text{ Er}^{3+}$  ions/ $\text{m}^3$  and  $8.6 \times 10^{26} \text{ Yb}^{3+}$  ions/ $\text{m}^3$ . These very high doping levels

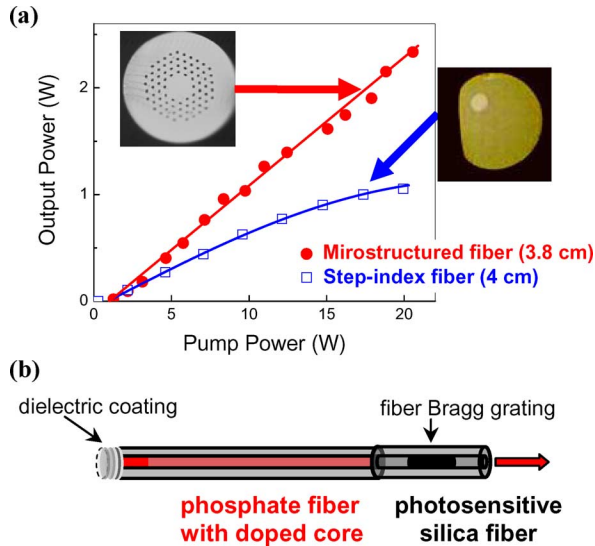


Fig. 4. (a) Comparison between the performances of single-frequency fiber lasers with conventional active step-index fiber and with a large core microstructure design, respectively. In both cases the laser cavity, shown in (b), is formed by a broadband dielectric mirror on the pump side and a narrowband Bragg grating for longitudinal mode selection on the fiber laser output side. Note that the better performing laser with MOF has an even shorter active fiber segment (3.8 versus 4 cm).

without the appearance of detrimental ion clustering effects have been achieved through a long optimization process of the active phosphate glasses.

The structures of both step-index and microstructured active fiber have been carefully optimized to maximize the absorption of multimode pump light (that is delivered through a multimode fiber with 105- $\mu\text{m}$  core diameter) while maintaining single-mode operation at the signal wavelength [17]. Clearly, the large, single-mode core of the MOF ( $\sim 430 \mu\text{m}^2$ ) results in an improved performance. The combination of large mode fiber design and high doping results in extremely efficient absorption of the cladding launched pump light with less than 20% pump transmitted through the active MOF of 3.8-cm length. With the MOF, an optical-to-optical conversion efficiency of  $\sim 12\%$  is observed up to pump powers of 20 W. This efficiency is more than twice as high as the maximum conversion efficiency of  $\sim 5\%$  of the single-frequency fiber laser that uses conventional step-index fiber. In addition, the step-index fiber lasers showed strong saturation effects at pump levels above 10 W. Due to saturation, the optical conversion efficiency of step-index fiber lasers decreases below the 5% level at higher pump powers. A maximum single-frequency output power over 2.3 W demonstrates the advantages of the phosphate MOF-based laser device over the conventional step-index fiber laser with a saturated maximum output power of 1.6 W that was achieved at pump levels above 35 W [16]. As already indicated above, a small price has to be paid in terms of mode quality. Although the laser operates in a single transverse mode, the measured mode quality factor  $M^2$  is approximately 1.2, which is slightly higher than unity due to deviations of the mode shape from a circular symmetric Gaussian intensity distribution. To achieve these modal properties, we applied the recently introduced depressed-index core design that allows for single-mode operation at relaxed tolerances for refractive index control [12]. The active phosphate

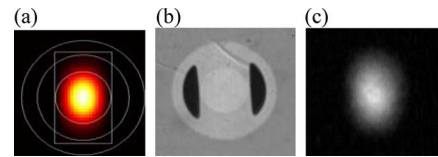


Fig. 5. (a) Eigenmode of the designed active birefringent fiber calculated using commercial software by photon design. (b) Cross-sectional image of the fabricated fiber zooming in on the area around the active core (bright central area) with air holes (dark areas) in close vicinity to the core. (c) Mode profile measured 63 cm from a fiber laser output facet using the birefringent fiber with doped phosphate glass core.

MOF had an air hole period of 8  $\mu\text{m}$ , air hole diameters of about 3.2  $\mu\text{m}$ , and a nominal index difference between core and cladding glasses of  $\Delta n = n_{\text{core}} - n_{\text{clad}} = -17 \times 10^{-4}$ .

#### IV. PHOSPHATE FIBERS WITH MICROSTRUCTURE-INDUCED BIREFRINGENCE

A highly desirable feature for many applications is the guidance of light while maintaining its polarization state. This property is traditionally achieved by breaking the circular symmetry of a fiber and the guided mode of a single-mode fiber becomes birefringent if the fiber is intentionally made twofold symmetric. Traditional polarization maintaining fiber, such as panda or bow-tie types, contain different glasses with different thermal properties, a characteristic that can be detrimental in particular in applications where considerable heat is generated such as fiber amplifiers and lasers.

An alternative approach is to design a microstructured fiber with structural birefringence [18]–[20]. Such structural birefringence can be an order of magnitude higher than the stress-induced birefringence in conventional polarization maintaining step-index fibers. Even absolutely single-polarization fiber has been developed utilizing the enormous design flexibility of microstructured fibers [21]–[23]. These single-polarization fibers guide only one polarization state in a specific range of wavelength. Therefore, both polarization mode coupling and polarization mode dispersion are eliminated.

The application of polarization maintaining and single-polarization fiber can significantly improve the stability and performance of fiber optic devices. In the following, we will describe our efforts to utilize fiber structuring techniques for the fabrication of birefringent active phosphate fiber. These fibers can be applied to build fiber lasers with birefringent fundamental modes and single-polarization lasers.

##### A. Active Polarization Maintaining Fiber

In many laser applications, single-polarization emission is required. To achieve this characteristic, it is not always necessary but highly beneficial to have active fibers that are polarization maintaining or, even better, support only one polarization state at the signal wavelength while the orthogonal polarization state experiences high losses. Therefore, we designed and fabricated a birefringent active phosphate glass fiber that is shown in Fig. 5. With two large air holes in close vicinity of the core, the fiber design is similar to recently demonstrated single-polarization fibers [21], [22]. However, our design features a circular

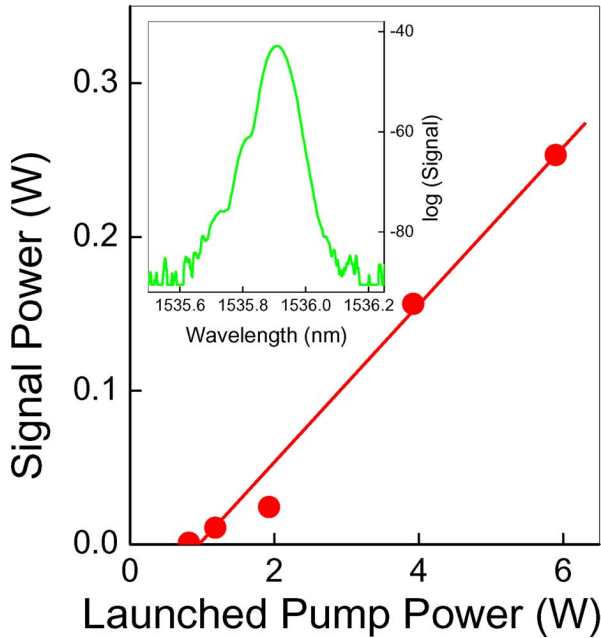


Fig. 6. Signal versus launched pump power for a single-polarization fiber laser using 24 cm of the active birefringent fiber shown in Fig. 4(a). A commercial FBG in PM fiber and a broadband reflector at the pump side form a cavity similar to that illustrated in Fig. 4(b). Inset: single-polarization fiber laser output spectrum.

core resulting in a more circular fundamental mode that is presented in the calculated and measured modes profiles shown in Fig. 5(a) and (c). There still remains a tradeoff between the degree of birefringence and the deviation of the mode from circular symmetry. In contrast to previous designs, in our case, both the calculated and the measured mode shapes closely resemble a Gaussian profile in both vertical and horizontal directions, but there still is a difference in the mode waist; the vertical waist is about 50% larger than the horizontal one. Our fiber features a 9- $\mu\text{m}$  core with a refractive index of 1.574, an inner cladding with a refractive index of 1.5706 and a diameter of 20  $\mu\text{m}$ , and an outer cladding with a refractive index of 1.556 and a diameter of 125  $\mu\text{m}$ . All indices are measured at 1.55  $\mu\text{m}$ .

The inner cladding contains two air holes on opposite sides of the core that get as close as  $\sim 0.1$   $\mu\text{m}$  to the core in the vertical direction and extend to a maximum distance of 7.5  $\mu\text{m}$  from the fiber center. The presence of these air holes results in a difference in the modal indices for the two orthogonal polarization states of  $\Delta n = 9 \times 10^{-5}$  at 1.55  $\mu\text{m}$ , however, both polarization modes can be supported inside the core. This birefringence value is about three times smaller than that of commercial polarization maintaining fiber. One of the advantages of this microstructured design with close-to-core air holes is the potential to control the fiber birefringent by filling the voids with different materials [24], a characteristic that might be exploited in both laser and sensing applications that utilize environmentally dependent birefringence as the test parameter.

In Fig. 6, we demonstrate the possibility of utilizing the birefringent fiber as gain medium in a single-polarization fiber laser. The core of the fiber [see Fig. 5(b)] is codoped with Er and Yb at levels of  $1.6 \times 10^{26}$   $\text{Er}^{3+}$  ions/ $\text{m}^3$  and  $8.6 \times 10^{26}$   $\text{Yb}^{3+}$  ions/ $\text{m}^3$

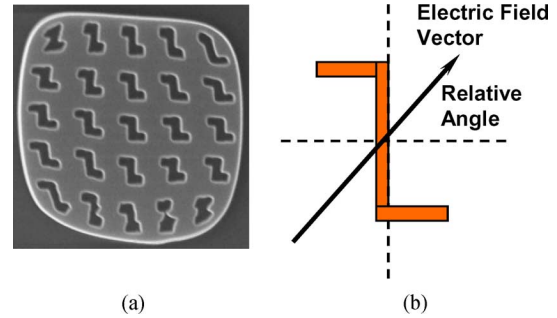


Fig. 7. (a) SEM image of a fiber facet. Shown is the area around the 5.2  $\mu\text{m} \times 5.2$   $\mu\text{m}$  core that comprises two different glasses arranged in a pattern with feature sizes smaller than the wavelength of light. (b) Experimental configuration for the birefringence measurement.

to provide gain at 1.55  $\mu\text{m}$  when pumped at 980 nm. The laser demonstrated in Fig. 6 contains a 24-cm-long active PM-fiber segment that is spliced to a commercial PM-FBG (PM-050-5-12993, OE/LAND) and is pumped by a fiber-coupled multi-mode pump laser. Similar to the fiber laser geometry shown in Fig. 4(b), a broadband dielectric coating on the pump side serves as the second cavity mirror, while the facet of the output fiber with FBG is angle cleaved. Laser emission at levels up to  $\sim 250$  mW was observed with a narrow spectral bandwidth determined by the FBG reflection spectrum. The output beam is linearly polarized with an extinction ratio over 22 dB. It should be noted that it is very difficult to achieve highly reliable and repeatable splicing between the active fiber with air holes and the PM-FBG fiber. This technical difficulty presently limits the achievable output power of this single-polarization fiber laser, but does not present a principal limitation for the application of birefringent or single-polarization active fibers.

### B. Birefringence Induced by Subwavelength Dielectric Structures Inside a Fiber Core

Considering the tradeoff between mode field distribution and structural birefringence in MOFs, alternatives are sought for highly birefringent fibers that allow for mode fields compatible with conventional optical fibers. One explored road combines microstructures and stress rods similar to conventional panda or bow-tie designs [23], [24]. Here we propose and explore a different approach based on the incorporation of a periodic dielectric structure directly into the core. Fabricating cores with subwavelength modulations of the refractive index results in the creation of a birefringent effective medium that forms the fiber core. This approach allows for a clear decoupling of the mode field design through an effective index structure and the design of birefringence through subwavelength structure engineering.

We test this approach using a phosphate glass fiber that has a standard outer diameter of 125  $\mu\text{m}$  and a small, almost square core with a size of 5.2  $\mu\text{m} \times 5.2$   $\mu\text{m}$ . A SEM image of the fiber core is shown in Fig. 7(a). The core consists of a dielectric structure fabricated using two glasses that are visible as light and dark regions, respectively. The refractive indices of the two core glasses are rather different, 1.559 and 1.574, respectively, at 1.55  $\mu\text{m}$ . The cladding has an index of 1.554 resulting in an effective V number of 1.29 for this fiber and a near-Gaussian single-mode guidance at 1.55  $\mu\text{m}$ .

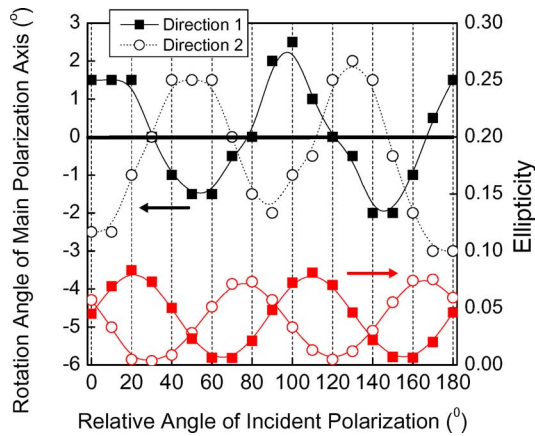


Fig. 8. Angle of rotation of the principal polarization axis (left) and ellipticity (right) after propagation through 8 cm of fiber with subwavelength dielectric core pattern. In any case, the incident light had a linear polarization with less than 0.01 ellipticity. Both observables are plotted as a function of the relative angle between the polarization of the incident light and the orientation of the nanostructure axis. Squares and circles are experimental data while lines are drawn to guide the eye.

The subwavelength structure inside the core was intended to be a periodic arrangement of 25 identical units with a periodicity of  $\sim 1 \mu\text{m}$ . Although the final arrangement inside the fiber core is slightly distorted after the fabrication process, there clearly remains a distinction between the vertical and the horizontal direction as opposed to a random distribution of the orientation of individual units.

To study how the complex nanostructure affects the polarization state during propagation we investigate its effect upon linearly polarized light launched into the core of this fiber. A schematic of the experimental conditions is shown in Fig. 7(b). Linearly polarized light is launched into the fiber core with an electric field vector forming a relative angle with the orientation of the subwavelength structures. After propagation through an 8-cm segment of this specialty fiber, two parameters are measured and plotted in Fig. 8. The first parameter, referring to the right axis, is the ellipticity of the polarization state of light after exiting the specialty fiber segment. The second parameter, linked to the left axis, is the relative angular rotation of the major polarization axis (compared with the incident polarization) after propagation. Since individual subwavelength structures are of chiral nature, we performed the same experiment with light launched from either side of the fiber.

The experimental results shown in Fig. 8 can be understood as follows. 1) Quantitatively, the fiber affects the light propagation in exactly the same way as any birefringent linear retarder, i.e., as a conventional birefringent fiber such as a panda fiber that has been tested with the same setup. 2) The two principal axes are tilted by  $\sim 30^\circ$  with respect to the horizontal and vertical axis of the image in Fig. 7(a). This can be directly seen considering the data of Fig. 8. If light is launched with polarization along either one of these two principal axes, no ellipticity is acquired and the polarization axis is not rotated. 3) There is no difference in the polarization effects when launching the light from one side or the other. All measurements are symmetric relative to the zero angles along both the fiber directions. 4) The measurements can

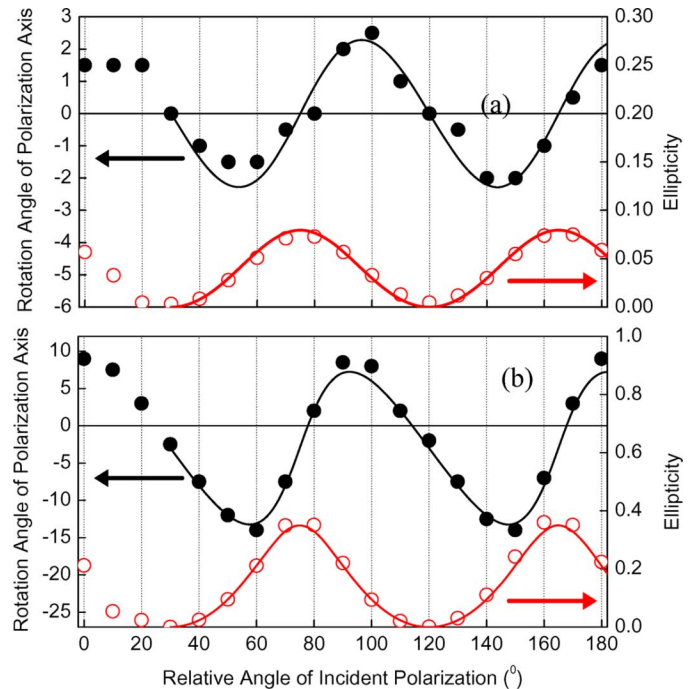


Fig. 9. Comparison between experimental and simulated polarization data for propagation through (a) an 8-cm-long fiber segment and (b) a 16-cm-long fiber segment. Circles are experimental data and lines represent best fits assuming phase delays  $\Delta\Phi$  of 0.55 and 1, respectively, for field components along the polarization axes. Note the different vertical scales in (a) and (b).

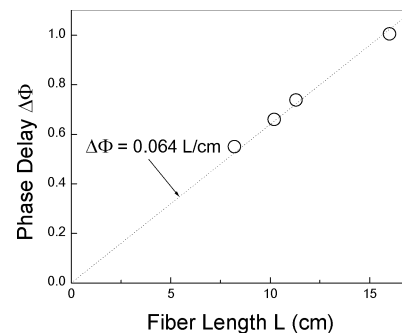


Fig. 10. Observed phase retardation as a function of the length of the specialty fiber segment.

be quantitatively reproduced in very good agreement assuming linear phase retardation between the two orthogonal axes characterized by two different phase velocities or refractive indices for the respective field components.

This is demonstrated in Fig. 9 where fits of the experimental data are shown for propagation through fiber segments of two different lengths. The sole parameter adjusted to obtain the closest match is the phase retardation  $\Delta\Phi$  characteristic for the particular fiber segment. Very good matches have been found for various fiber lengths. Fig. 10 summarizes the obtained phase delays as a function of fiber length. In good approximation, we observed a linear dependence and can conclude that our specialty fiber has a birefringence of  $\Delta\beta = (0.064 \pm 0.001)/\text{cm}$ , corresponding to a refractive index difference of  $\Delta n \sim 1.5 \times 10^{-6}$  between the two axis. This value has to be compared to  $\Delta n \sim 3 \times 10^{-4}$  for commercial

birefringent, polarization maintaining fiber. The corresponding beat length of our fiber is  $L_B = 2\pi/\Delta\beta \sim 1$  m. The demonstrated birefringence might be small, but this first attempt should be considered a starting point for optimizing individual features, their arrangement, and the materials to make this concept useful for practical applications.

Detailed experimental studies are ongoing to establish understanding of the origin and magnitude of the induced birefringence on a microscopic level. This knowledge is necessary to gain predictable capabilities and fabricate fibers with subwavelength structures for applications such as fiber optic wave plates. However, these first findings clearly reveal exciting possibilities for future fiber devices. The ability to fabricate artificial effective media inside the core of an optical fiber creates a whole set of new tools for design and engineering of optical fibers.

## V. CONCLUSION

We have demonstrated the fabrication of high-quality MOF made of phosphate glass. Large core MOFs have been applied to enhance the performance of phosphate glass fiber lasers. The fabrication technique can also be used to induce structural birefringence. Active birefringent MOFs can improve the stability of single-polarization fiber lasers. We also show that birefringence can be achieved through periodic arrangements of subwavelength dielectric units inside the fiber core. The demonstrated feasibility of incorporating various materials with subwavelength features into the core of an optical fiber opens new routes for advanced fiber designs and even more functionality of future fiber devices.

## ACKNOWLEDGMENT

The authors would like to thank Y. Merzlyak and E. Temyanko for technical support and H. Li and E. M. Wright for stimulating discussions.

## REFERENCES

- [1] J. C. Knight, T. A. Birks, P. S. J. Russell, and D. M. Atkin, "All-silica single-mode fiber with photonic crystal cladding," *Opt. Lett.*, vol. 21, pp. 1547–1549, 1996.
- [2] P. S. J. Russell, "Photonic crystal fibers," *Science*, vol. 299, pp. 358–362, 2003.
- [3] T. A. Birks, J. C. Knight, and P. S. J. Russell, *Opt. Lett.*, vol. 22, pp. 961–963, 1997.
- [4] J. C. Knight, T. A. Birks, R. F. Cregan, P. S. J. Russell, and J.-P. de Sandro, "Large mode area photonic crystal fiber," *Electron. Lett.*, vol. 34, pp. 1347–1348, 1998.
- [5] J. C. Knight, J. Broeng, T. A. Birks, and P. S. J. Russell, "Photonic bandgap guidance in optical fibers," *Science*, vol. 282, pp. 1476–1478, 1998.
- [6] W. J. Wadsworth, J. C. Knight, W. H. Reeves, P. S. J. Russell, and J. Arriaga, "Yb<sup>3+</sup>-doped photonic crystal fibre laser," *Electron. Lett.*, vol. 36, pp. 1452–1454, 2000.
- [7] T. M. Monro, Y. D. West, D. W. Hewak, N. G. R. Broderick, and D. J. Richardson, "Chalcogenide holey fibers," *Electron. Lett.*, vol. 36, pp. 1998–2000, 2000.
- [8] V. V. Ravi Kanth Kumar, A. K. George, W. H. Reeves, J. C. Knight, P. S. J. Russell, F. G. Omenetto, and A. J. Taylor, "Extruded soft glass photonic crystal fiber for ultrabroad supercontinuum generation," *Opt. Exp.*, vol. 10, pp. 1520–1525, 2002.
- [9] X. Feng, A. K. Mairaj, D. W. Hewak, and T. M. Monro, "Nonsilica glasses for holey fibers," *J. Lightw. Technol.*, vol. 23, no. 6, pp. 2046–2054, Jun. 2005.

- [10] J. Limpert, T. Schreiber, S. Nolte, H. Zellmer, T. Tünnemann, R. Iliw, F. Lederer, J. Broeng, G. Vienne, A. Petersson, and C. Jakobsen, "High-power air-clad large-mode-area photonic crystal fiber laser," *Opt. Exp.*, vol. 11, pp. 818–823, 2003.
- [11] L. Li, A. Schülzgen, V. L. Temyanko, T. Qiu, M. M. Morrell, Q. Wang, A. Mafi, J. V. Moloney, and N. Peyghambarian, "Short-length microstructured phosphate glass fiber lasers with large mode areas," *Opt. Lett.*, vol. 30, pp. 1141–1143, 2005.
- [12] L. Li, A. Schülzgen, V. L. Temyanko, S. Sabet, M. M. Morrell, H. Li, A. Mafi, J. V. Moloney, and N. Peyghambarian, "Investigation of modal properties of microstructured optical fibers with large depressed-index cores," *Opt. Lett.*, vol. 30, pp. 3275–3277, 2005.
- [13] L. Li, A. Schülzgen, V. L. Temyanko, M. M. Morrell, S. Sabet, H. Li, J. V. Moloney, and N. Peyghambarian, "Ultra-compact cladding-pumped 35-mm-short fiber laser with 4.7-W single-mode output power," *Appl. Phys. Lett.*, vol. 88, 2006, 161106.
- [14] A. Schülzgen, L. Li, V. L. Temyanko, S. Suzuki, J. V. Moloney, and N. Peyghambarian, "Single-frequency fiber oscillator with watt-level output power using photonic crystal phosphate glass fiber," *Opt. Exp.*, vol. 14, pp. 7087–7092, 2006.
- [15] J. Limpert, A. Liem, M. Reich, T. Schreiber, S. Nolte, H. Zellmer, A. Tünnemann, J. Broeng, A. Petersson, and C. Jakobsen, "Low-nonlinearity single-transverse-mode ytterbium-doped photonic crystal fiber amplifier," *Opt. Exp.*, vol. 12, pp. 1313–1319, 2004.
- [16] T. Qiu, S. Suzuki, A. Schülzgen, L. Li, A. Polynkin, V. Temyanko, J. V. Moloney, and N. Peyghambarian, "Generation of watt-level single longitudinal mode output from cladding pumped short fiber lasers," *Opt. Lett.*, vol. 30, pp. 2748–2750, 2005.
- [17] T. Qiu, L. Li, A. Schülzgen, V. L. Temyanko, T. Luo, S. Jiang, A. Mafi, J. V. Moloney, and N. Peyghambarian, "Generation of 9.3-W multimode and 4-W single-mode output from 7-cm short fiber lasers," *IEEE Photon. Technol. Lett.*, vol. 16, no. 12, pp. 2592–2594, Dec. 2004.
- [18] A. Ortigosa-Blanch, J. C. Knight, W. J. Wadsworth, B. J. Mangan, T. A. Birks, and P. S. J. Russell, "Highly birefringent photonic crystal fibers," *Opt. Lett.*, vol. 25, pp. 1325–1327, 2000.
- [19] M. J. Steel and R. M. Osgood Jr., "Elliptical-hole photonic crystal fibers," *Opt. Lett.*, vol. 26, pp. 229–231, 2001.
- [20] T. P. Hansen, J. Broeng, S. E. B. Libori, E. Knudsen, A. Bjarklev, J. R. Jensen, and H. R. Simonsen, "Highly birefringent index-guiding photonic crystal fibers," *IEEE Photon. Technol. Lett.*, vol. 13, no. 6, pp. 588–590, Jun. 2001.
- [21] H. Kubota, S. Kawanishi, S. Koyanagi, M. Tanaka, and S. Yamaguchi, "Absolutely single polarization photonic crystal fiber," *IEEE Photon. Technol. Lett.*, vol. 16, pp. 182–184, 2004.
- [22] D. A. Nolan, G. E. Berkey, M.-J. Li, X. Chen, W. A. Wood, and L. A. Zenteno, "Single-polarization fiber with a high extinction ratio," *Opt. Lett.*, vol. 29, pp. 1855–1857, 2004.
- [23] J. R. Folkenberg, M. D. Nielsen, and C. Jakobsen, "Broadband single-polarization photonic crystal fiber," *Opt. Lett.*, vol. 30, pp. 1446–1448, 2005.
- [24] Kerbage and B. J. Eggleton, "Numerical analysis and experimental design of tunable birefringence in microstructured optical fiber," *Opt. Exp.*, vol. 10, pp. 246–255, 2002.

**Axel Schülzgen** received the Ph.D. degree in experimental physics from Humboldt University, Berlin, Germany, in 1992.

During 1992–1995, he was a Research Fellow at Trinity College, Dublin, Ireland, and at Humboldt University Berlin, and studied optical properties of low-dimensional semiconductor quantum structures. In 1996, he joined the University of Arizona, Tucson, where he currently works as a Research Professor at the College of Optical Sciences. His work focuses on the investigation of advanced micro- and nanostructured materials, novel nonlinear optical effects, ultrafast optics, and laser development.

**Li Li** received the M.A. degree in physics from Wayne State University, Detroit, MI, in 2001 and the Ph.D. degree in optical sciences from the University of Arizona, Tucson, in 2005.

He then joined the College of Optical Sciences, University of Arizona, as a Research Associate and later an Assistant Research Scientist from 2005 to 2008. He is currently with TIPD LLC, Tucson, AZ, as an Optical Engineer. His current research interests are in the field of novel optical fibers and silicon-on-insulator-based integrated optoelectronic devices.

**Xiushan Zhu** received the B.S. degree in physics and the M.S. degree on optical information processing from Nankai University, Tianjin, China, in 1996 and 1999, respectively, and the M.S. degree in fiber devices from the University of New Mexico, Albuquerque, in 2004. Currently, he is working towards the Ph.D. degree in the area of fiber lasers and amplifiers at the University of Arizona, Tucson.

During 1999–2001, he was an Optical Engineer at Wuhan Research Institute of Telecommunications and Posts, Wuhan, China, where he was engaged in research of erbium-doped fiber amplifiers (EDFAs) and passive fiber devices for optical communications. At the University of New Mexico, his work focused on an all-fiber polarization transformer, mid-infrared fiber lasers and amplifiers, and stimulated Brillouin scattering in optical fibers. His current research interests include polarization states of laser arrays, fiber lasers and amplifiers based on multimode interference, narrow-linewidth mid-infrared fiber lasers, and nanostructured fibers.

**Valery L. Temyanko** received the M.S. degree in chemical engineering from Louisiana State University, Baton Rouge, in 1997.

In 2000, he joined the University of Arizona, Tucson, where he is a Staff Engineer. His research activities include manufacturing of micro- and nanostructured fibers, fiber lasers, electro-optic modulators, couplers, and switches.

**Nasser Peyghambarian** (M'03) received the Ph.D. degree in physics from Indiana University, Bloomington, in 1982.

His research interests include optical telecommunication, fiber optics, fiber amplifiers and fiber lasers, integrated optics including waveguide amplifiers, lasers, modulators; femtosecond laser spectroscopy and dynamics of optical phenomena in semiconductors and organic materials; nonlinear photonics and high-speed optical switching; characterization of optical materials in terms of speed and nonlinearities; polymer optoelectronics, photorefractive polymers, organic light emitting diodes and lasers.

Dr. Peyghambarian is a fellow of the American Physical Society, the Optical Society of America (OSA), and The International Society for Optical Engineers (SPIE).